

Circular RABBITT goes under threshold

Vladislav V. Serov¹, Jia-Bao Ji², Meng Han³, Kiyoshi Ueda^{4,5}, Hans Jakob Wörner², and Anatoli S. Kheifets⁶

¹Department of Medical Physics, Saratov State University, Saratov 410012, Russia

²Laboratorium für Physikalische Chemie, ETH Zürich, 8093 Zürich, Switzerland

³J. R. Macdonald Laboratory, Department of Physics,
Kansas State University, Manhattan, KS 66506, USA

⁴Department of Chemistry, Tohoku University, Sendai, 980-8578, Japan

⁵School Physical Science and Technology, ShanghaiTech University, Shanghai 201210, China and

⁶Research School of Physics, The Australian National University, Canberra ACT 2601, Australia*

(Dated: June 10, 2025)

We utilize the process of Reconstruction of Attosecond Beating By Interference of Two-photon Transitions (RABBITT) driven by circularly polarized radiation to map under-threshold discrete excitations in noble gas atoms. Great advantage of circular polarization is that it allows to reach selectively various angular components of the photoelectron wavepacket and to resolve two-photon ionization amplitudes including their phases. By doing so, we picture resonant two-photon ionization in an unprecedented detail not seen previously. In particular, we break, with high confidence, the Fano propensity rule formulated for two-photon ionization by Busto *et al* [Phys. Rev. Lett. **123**, 133201 (2018)]. We also demonstrate a great utility of the Coulomb Green's function approach proposed by Krylovetsky *et al* [Sov. Phys. – JETP **92**, 37 (2001)] more than two decades ago.

PACS numbers: 32.80.Rm 32.80.Fb 42.50.Hz

Two-photon XUV+IR ionization of atomic and molecular targets has been a powerful driver of attosecond science [1–3] facilitating its recent award of the Nobel Prize in Physics [4]. The technique of Reconstruction of Attosecond Beating By Interference of Two-photon Transitions (RABBITT) [5, 6] is one of the pillars of attosecond metrology. This technique offers convenient means to resolve atomic and molecular ionization processes in time and it has been particular beneficial for studying resonant two-photon ionization [7–14]. In most RABBITT applications, the XUV and IR pulses are co-linearly polarized. More recently, RABBITT with circularly polarized XUV and IR radiation, has been suggested [15] and then successfully implemented [16–18].

Common to all the RABBITT applications is a comb of odd XUV harmonics $(2q \pm 1)\omega$ from an attosecond pulse train (APT) which is augmented by an absorption or emission of one driving laser IR photon with the carrier frequency ω . This IR photon absorption/emission creates sidebands (SBs) centered at $2q\omega$ as illustrated in the photoelectron spectrum exhibited in Fig. 1a. The height of the sidebands oscillates at twice the IR photon frequency as the XUV/IR pulse delay τ varies:

$$S_{SB}(\tau) = A + B \cos[2\omega\tau - C] \quad , \quad C = 2\omega\tau_a \quad . \quad (1)$$

Here A, B are the RABBITT magnitude parameters and C is its phase. The latter is directly linked with the atomic time delay $\tau_a = \tau_W + \tau_{cc}$ decomposed into the Wigner time delay τ_W and the continuum-continuum (CC) component τ_{cc} [19].

If one harmonic energy submerges below the ionization threshold $(2q-1)\omega < |E_i| < (2q+1)\omega$, the corresponding

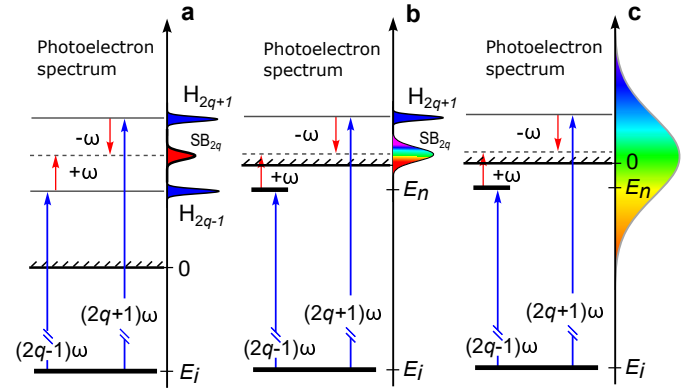


FIG. 1: Graphical illustration of the conventional (a) and the under-threshold (b,c) RABBITT processes. Rainbow SB spectral analysis is highlighted in (b). Continuously rainbow RABBITT is visualized in (c).

harmonic peak H_{2q-1} disappears from the photoelectron spectrum. Instead, the missing absorption path of the conventional RABBITT process can proceed via a series of discrete Rydberg excitations $E_n < 0$. Such an under-threshold or uRABBITT process is illustrated graphically in Fig. 1b. The uRABBITT process has been observed experimentally in He [12, 20–23], Ne [24] and Xe [25]. Theoretically, it has also been studied in Ne [26, 27] and Ar [28].

With circular radiation, the RABBITT parameters entering Eq. (1) become dichroic, i.e. they differ for the co-rotating (CO) and counter-rotating (CR) XUV and IR fields. The knowledge of the dichroic phase C in both cases allows for a retrieval of the two-photon ionization amplitudes and their phases. More specifically, the circular XUV photon absorption with $M = 1$ drives the initial atomic state $l_i, m_i \geq l_i - 1$ to the uniquely defined intermediate state with $\ell = l_i + 1$. Depending on the CR or

*Electronic address: A.Kheifets@anu.edu.au

CO polarization of the IR photon, the angular momentum of the final state acquires the two values $L = \ell \pm 1$. The set of the two CO/CR phases allows to determine the moduli ratio of the two ionization amplitudes and their relative phase [29, 30]

$$R_\ell^\pm = \left| T_{\ell \rightarrow \ell-1}^\pm / T_{\ell \rightarrow \ell+1}^\pm \right|, \quad \Delta\Phi_\ell^\pm = \arg \left[T_{\ell \rightarrow \ell-1}^\pm / T_{\ell \rightarrow \ell+1}^\pm \right] \quad (2)$$

The moduli ratios R_ℓ^\pm are of particular interest because of the recently formulated Fano propensity rule in two-photon XUV+IR ionization processes [31]. By virtue of this rule, the angular momentum is preferably increased or decreased in the IR photon absorption/emission processes, respectively. This implies the inequalities $R_\ell^+ < 1$ and $R_\ell^- > 1$. These inequalities have indeed been confirmed by numerical circular RABBITT (cRABBITT) simulations [29, 30]. Various analytic theories [32–35] do also generally support the Fano rule in two-photon ionization. However, at a sufficiently high IR photon frequency, a large orbital momentum of the target and a low photoelectron energy, a departure from the Fano propensity rule is predicted [34] with the CR polarization being able to produce $R_\ell^+ > 1$. At the photoelectron energies in between the two regimes of $R_\ell^+ < 1$ and $R_\ell^+ > 1$, the absorption ratio passes through a characteristic Cooper-like minimum.

These analytic predictions are hard to verify either numerically or experimentally because sufficiently low photoelectron energies always imply the uRABBITT regime. So the circular RABBITT should necessarily go under threshold. In this Letter, we demonstrate such a circular under threshold RABBITT (cuRABBITT). In this demonstration we employ a rainbow spectral analysis which is illustrated graphically in Fig. 1b. In the rainbow RABBITT (rRABBITT), each of the dense grid of energy points in the photoelectron spectrum under the SB_{2q} is the subject of the time variation (1) instead of the overall peak height as in Fig. 1a. Such an extended spectral analysis has proven instrumental to disentangle various ionization pathways involving autoionizing resonances [7, 9, 36, 37], below threshold discrete states [12] and fine-structure splittings [11, 38]. The same technique is beneficial when the presence of multiple ionization channels leads to spectral congestion in atoms [39] and molecules [40].

The restriction of the rRABBITT is that the useful data set is limited to the spectral width of the single above-threshold SB_{2q} . To span a sufficiently wide portion of the photoelectron spectrum, the IR photon energy ω should be continuously adjusted. This is not permitted in the present context as the ratios R_ℓ^\pm also change rapidly with ω . To circumvent this difficulty, we realize the continuous rRABBITT which is not limited to any particular SB. To this end, we replace a narrow-band APT with a short single attosecond pulse (SAP) thus producing a broad spectrum overlapping with an extended interval of the photoelectron energies as illustrated in Fig. 1c. This photoelectron spectrum is strongly dominated by

single XUV photon ionization. To enhance two-photon ionization and to deduce the parameters of the cosine $2\omega\tau$ oscillation in Eq. (1), we subtract the single-photon ionization component from the total ionization amplitude thus bringing out the net two-photon ionization contribution. An alternative and more general enhancement method is based on the parity separation of the single-photon and two-photon ionization processes. In the case of an atom or a symmetric molecule, the two-photon ionization amplitude has the same parity as the initial state of the target while the single-photon ionization amplitude has an opposite parity. Hence, the two-photon ionization can be effectively isolated by performing the amplitude symmetrization $A(\mathbf{k}) + (-1)^p A(-\mathbf{k})$, where parity $p = l_i$ for a closed-shell atom.

Our computer simulations have been conducted by solving numerically the time-dependent Schrödinger equation (TDSE) in the single active electron approximation. The two independently developed computer codes [41, 42] were used for cross-checking. The TDSE is driven by the vector potential $\mathbf{A}(t)$ which includes both the XUV and IR fields. The XUV field is represented by a Gaussian pulse $A_x(t) = A_0 \exp(-2 \ln 2 t^2 / \tau_x^2) \cos \omega_x t$. Here A_0 is the vector potential peak value and the central frequency ω_x is chosen close to the ionization threshold of the atom under consideration. The IR pulse has a cosine squared envelope shifted from the center of the XUV pulse by a variable delay τ which is incremented in several steps. Unlike the attosecond streak camera, which also utilizes SAP [43], both the XUV and IR intensities are kept low in the 10^{10} W/cm² range to retain the ionization process within the lowest order of perturbation theory (LOPT). The photoelectron spectrum in the given emission direction is obtained by using the surface flux method [44–46]. The angular and energy resolved RABBITT parameters are deduced by projecting the time oscillation signal (1) on the unity, $\cos 2\omega t$ and $\sin 2\omega t$ basis. The amplitude ratios and the phase differences (2) are obtained by fitting the angular dependent RABBITT phase $C(\theta)$ with the following expressions [29]

$$C_{l_i=0, m_i=0}^{\text{CR/CO}} \stackrel{\ell=1}{=} \arg \left[T_2^- T_2^{+*} \right] + \arg \left[P_2(\cos \theta) - \frac{T_0^\pm}{T_2^\pm} \right] \quad (3)$$

$$C_{l_i=1, m_i=0}^{\text{CR/CO}} \stackrel{\ell=2}{=} \arg \left[T_3^- T_3^{+*} \right] + \arg \left[\bar{P}_3(\cos \theta) - \frac{T_1^\pm}{T_3^\pm} \right].$$

Here CR/CO orientation corresponds to the $+/-$ signs and $\bar{P}_3^1 \equiv P_3^1 / P_1^1 = \frac{3}{2}(-1 + 5 \cos^2 \theta)$. Similar expressions can be derived for higher orbital momenta [30].

Results of our numeric simulations are exhibited in Fig. 2 which displays the moduli ratios $|T_{\ell-1}^\pm / T_{\ell+1}^\pm|$ (the top row) and the phase differences $\arg[T_{\ell-1}^\pm / T_{\ell+1}^\pm]$ (the bottom row) for He 1s (left, $\ell = 1$), Ar 3p (center, $\ell = 2$) and Xe 4d (right, $\ell = 3$). Here we choose the laser photon frequency in the 200 nm spectral range at $\omega = 6.09$ eV to span efficiently the whole manifold of the discrete target states. These states are revealed in the photoelectron spectrum at the energies $E_n + \omega$.

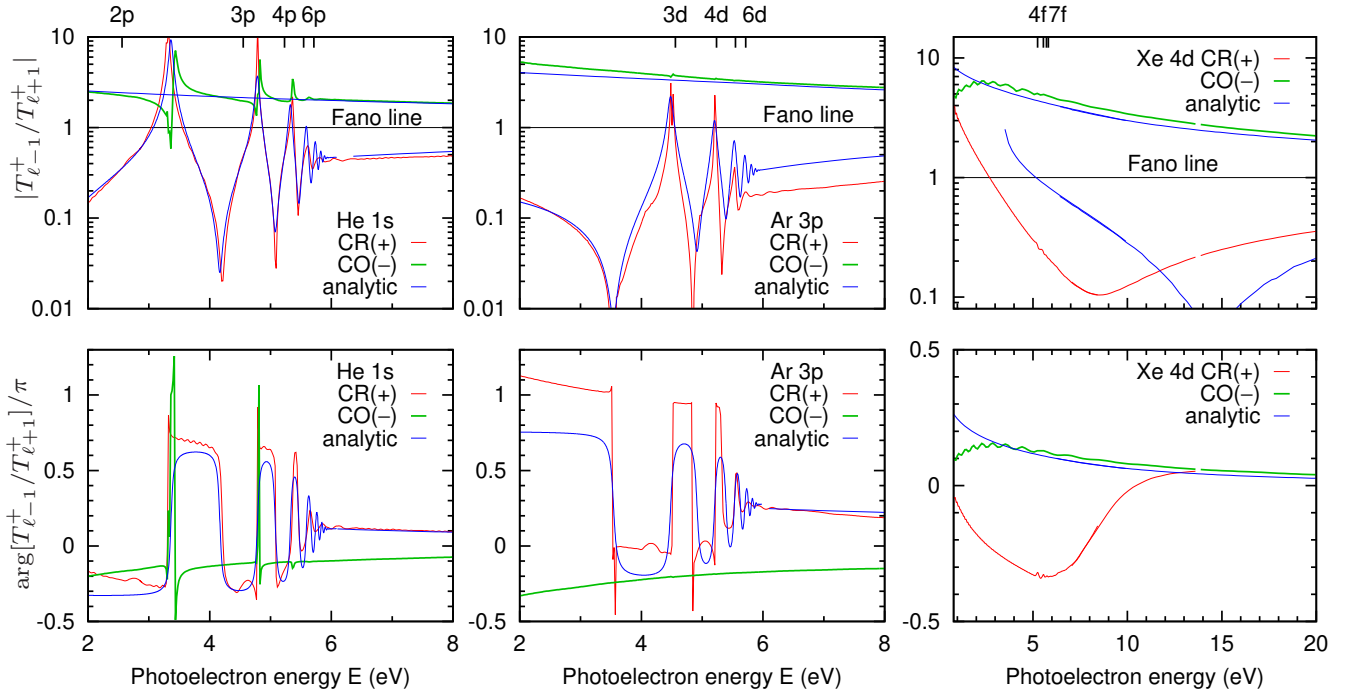


FIG. 2: The moduli ratio $|T_{\ell-1}^{\pm}/T_{\ell+1}^{\pm}|$ (top) and the phase difference $\arg[T_{\ell-1}^{\pm}/T_{\ell+1}^{\pm}]/\pi$ (bottom) for He 1s (left, $\ell = 1$), Ar 3p (center $\ell = 2$) and Xe 4d (right, $\ell = 3$). In the He and Ar cases, the modified Sturmian expansion is used to evaluate the singular term in Eq. (4). In the case of Xe, the analytic results of [34] extended continuously towards the threshold are plotted. Note a broadened photoelectron energy range in Xe allowing to visualize the Cooper minimum.

As expected from the uRABBITT diagrams of Fig. 1b and c, it is the absorption path of the RABBITT process that should probe the discrete under-threshold excitations most directly. In the circular RABBITT, the absorption path is encoded into the CR phase. So it is the complex amplitude ratio $T_{\ell-1}^{\pm}/T_{\ell+1}^{\pm}$ that should reveal the resonant structure most clearly and indeed we observe this structure with the CR orientation in He 1s and Ar 3p. In He, some weaker resonant structure is also present at the CO orientation.

In the top row of panels, we draw the Fano line $R = 1$ that divides the $R^- > 1$ and $R^+ < 1$ ratios provided they comply with the Fano propensity rule. The Fano line is crossed and the rule is broken in all the considered target atoms. In He, the line is crossed with both the CR and CO orientations while in Ar and Xe it is the CR orientation that breaks the Fano rule.

The strong resonant behavior seen in the cases of He 1s and Ar 3p can be interpreted qualitatively within the LOPT. In this framework, the two-photon ionization amplitudes can be presented as [19, 21]

$$T_{\ell}^{\pm}(E = k^2/2) \propto \frac{1}{i} \mathcal{E}_{\Omega} \mathcal{E}_{\omega} \left\{ \sum_{E_{n\ell} < 0} + \int_0^{\infty} d\kappa^2 \right\} (-i)^L e^{i\eta_L} \times \left[\frac{\langle kL \| r \| n\ell \rangle \langle n\ell \| r \| n_i l_i \rangle}{E_i + \Omega^{\pm} - E_{n\ell} - i\gamma} + \frac{\langle kL \| r \| \kappa\ell \rangle \langle \kappa\ell \| r \| n_i l_i \rangle}{E_i + \Omega^{\pm} - \kappa^2/2 - i\gamma} \right] \quad (4)$$

Here $\mathcal{E}_{\Omega}, \mathcal{E}_{\omega}$ are the spectral contents of the XUV and IR fields, respectively, while $\langle n_i l_i \|, \langle \kappa\ell \|$ and $\langle kL \|$ are the initial, intermediate and final electron states de-

fined by their linear and angular momenta. The first term in the second line of Eq. (4) describes the discrete excitations whereas the second term contains the continuum-continuum transitions. The first term becomes singular at the excitation energy $E_i + \Omega^+ = E_{n\ell}$. The second term remains regular and can be evaluated analytically [32–35]. As shown by Drescher et al. [21], the singular term manifests itself by the series of resonances and anti-resonances each accompanied by a π up and down phase jump. It is exactly this behavior that is seen in the phase diagrams of the bottom row of Fig. 2 in the cases of He (both the CR and CO) and Ar (CR only). Due to a much larger threshold energy, the Xe 4d ratios remain largely smooth. Here, the CR ratio displays a deep Cooper-like minimum and breaks the Fano line near the threshold as predicted in [34]. The only trace of discrete excitations can be observed in very minor oscillation of the CR phase.

Direct evaluation of the singular term in Eq. (4) is not practical as it is difficult to enforce a smooth transition over the threshold seen in our TDSE results. Instead, we adopt a combined approach. The singular term in Eq. (4), which is important in the absorption pathway, is evaluated using the modified Sturmian expansion of the Coulomb Green's function [47]. Meanwhile the regular term, which is dominant in the emission pathway, is dealt with as in the preceding work [34] by expressing the integrals of the confluent hypergeometric functions via the Appell F_1 function.

Our evaluation was performed in Python using the sci-

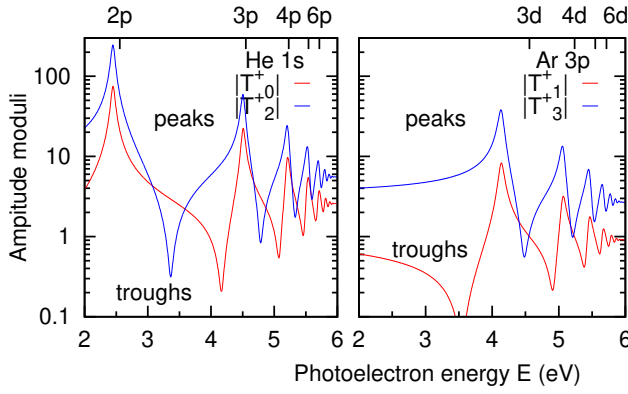


FIG. 3: Left: Peaks and troughs of the amplitudes $|T_{0+}^+|$ and $|T_{2+}^+|$ in He. Right: Same for the amplitudes $|T_{1+}^+|$ and $|T_{3+}^+|$ in Ar.

entific libraries [48, 49]. By using the formulae from [47], the explicit summation in Eq. (4) is avoided. The p -values considering a finite pulse duration were given by $-2p^{-2} = \Omega^+ + E_i - i\gamma$, with $\text{Re}\{p\} > 0$ and $\gamma = 10^{-3}$ was used. The energy displacement of Rydberg states between hydrogen and helium was accounted for by a quantum defect interpolated from the Rydberg series $n_{\text{eff}} = 1/\sqrt{-2(\Omega^+ + E_i)} + d$ with $d = 0.0667$ for He and 0.359 for Ar. The emission pathway was aligned to the absorption pathway with the same final kinetic energy.

Such an evaluation for the amplitudes (4) produces the moduli ratios which agree rather closely with the TDSE results for He and Ar as is seen in the top left and central panels of Fig. 2. There a slight offset in phases between the two methods which can be removed by lifting the hydrogenic phase by a small constant value. Then the phases match fairly closely as is seen in the bottom left and central panels of Fig. 2.

By validating the Coulomb Green's function approach, we can now look at the amplitudes $T_{\ell \rightarrow \ell-1}^+$ and $T_{\ell \rightarrow \ell+1}^+$ individually rather than at their ratio which is the only result of the numerical TDSE simulations. The moduli of the amplitudes $|T_{\ell \pm 1}^+|$ with $\ell = 1$ in He 1s and $\ell = 2$ in Ar 3p are displayed in the left and right panels of Fig. 3, respectively. As expected from Eq. (4), both pairs of amplitudes pass through the series of resonances and anti-resonances and display the set of peaks and troughs. Quite understandably, the resonant peaks of both the $\ell \rightarrow \ell \pm 1$ amplitudes match the same set of discrete energies shifted by the photon energy ω . However, quite remarkably, the anti-resonances and troughs are displaced between $\ell \pm 1$ amplitudes because of the different strength of the non-resonant continuum. This displacement brings about the strong oscillatory structure into the amplitude ratio $T_{\ell \rightarrow \ell-1}^+/T_{\ell \rightarrow \ell+1}^+$ as displayed in Fig. 2. Quite interestingly, the ratio becomes less oscillatory in Ar in comparison to He and all but flattens in Xe. In the latter atom, because of a considerably larger ionization threshold, the strengths of the two non-resonant continua equalize and the Cooper minimum further suppresses the resonant structure.

To summarize, we conduct a systematic investigation of discrete excitations in noble gas atoms using under-threshold circular RABBITT. By employing the rainbow spectral analysis combined with an ultrashort single XUV pulse, we are able to map these excitations continuously over an extended interval of photoelectron energies. Discrete under-threshold excitations manifest themselves as a series of resonances and anti-resonances detected with counter-rotating XUV and IR pulses. In the meantime, such a resonant structure is much weaker or absent with co-rotating ionizing and dressing XUV and IR fields.

We use our numerical TDSE simulations to validate the two analytic models. One such model employs the Coulomb Green's function [47] to evaluate the singular term in the lowest order perturbation theory expression (4) for the two-photon ionization amplitudes. The amplitude ratios and phase difference in He and Ar are found to be very close between the Green's function and TDSE calculations. This allows us to picture the individual two-photon ionization amplitudes in the two Es and Ed continua. Understandably, these amplitudes share the same resonant energies but quite surprisingly differ in location of their anti-resonances. This explains the strongly resonant behavior of the amplitude ratios which weakens from He to Ar and then almost wains in Xe.

Away from the resonance region, our moduli ratios and phase differences tend to predictions of the analytical model [34]. For target orbitals with large orbital momentum at small photoelectron energy, this model predicts existence of a Cooper-like minimum whose presence is confirmed in our numerical simulations. Below the minimum, the moduli ratio in the CR channel $|T_{\ell-1}^+/T_{\ell+1}^+|$ exceeds unity thus breaking the Fano propensity rule formulated for the two-photon XUV+IR ionization [31]. This rule, which favours increase of the orbital momentum with absorption of the IR photon, is also broken near the anti-resonances of the $T_{\ell+1}^+$ amplitude close to discrete under-threshold excitations.

The proposed combination of the rainbow spectral analysis and ultra-short XUV pulse utilization relies on an efficient enhancement of the two-photon ionization above normally much stronger single ionization background. This enhancement is achieved most effectively by a parity based symmetrization of the ionization amplitude. While the amplitude symmetrization is only possible in numerical experiments, the $\omega\tau$ oscillation which is characteristic to single IR photon absorption can be projected out in the experiment. This opens up a wider application of the proposed continuous rainbow RABBITT technique.

To conclude, we demonstrate feasibility of a novel continuously rainbow RABBITT technique with circular radiation which enriches the attosecond metrology and opens up a new direction for experimental and theoretical investigations.

Acknowledgment: This work is supported by the ARC Discovery Grant DP230101253. Resources of the National Computational Infrastructure have been utilized.

-
- [1] M. Hentschel, R. Kienberger, C. Spielmann, G. A. Reider, N. Milosevic, T. Brabec, P. Corkum, U. Heinzmann, M. Drescher, and F. Krausz, *Attosecond metrology*, Nature **414**, 509 (2001).
- [2] P. B. Corkum and F. Krausz, *Attosecond science*, Nature Phys. **3**, 381 (2007).
- [3] F. Krausz and M. Ivanov, *Attosecond physics*, Rev. Mod. Phys. **81**, 163 (2009).
- [4] P. Agostini, F. Krausz, and A. L’Huillier, *The Nobel Prize in Physics 2023*, NobelPrize.org (2023), awarded for their experimental methods that generate attosecond pulses of light to study electron dynamics in matter.
- [5] H. Muller, *Reconstruction of attosecond harmonic beating by interference of two-photon transitions*, Applied Physics B: Lasers and Optics **74**, s17 (2002), 10.1007/s00340-002-0894-8.
- [6] E. S. Toma and H. G. Muller, *Calculation of matrix elements for mixed extreme-ultraviolet-infrared two-photon above-threshold ionization of argon*, J. Phys. B **35**(16), 3435 (2002).
- [7] V. Gruson, L. Barreau, Á. Jiménez-Galan, F. Risoud, J. Caillat, A. Maquet, B. Carré, F. Lepetit, J.-F. Hergott, T. Ruchon, et al., *Attosecond dynamics through a Fano resonance: Monitoring the birth of a photoelectron*, Science **354**(6313), 734 (2016).
- [8] C. Cirelli, C. Marante, S. Heuser, C. L. M. Petersson, A. J. Galán, L. Argenti, S. Zhong, D. Busto, M. Isinger, S. Nandi, et al., *Anisotropic photoemission time delays close to a Fano resonance*, Nature Comm. **9**, 955 (2018).
- [9] D. Busto, L. Barreau, M. Isinger, M. Turconi, C. Alexandridi, A. Harth, S. Zhong, R. J. Squibb, D. Kroon, S. Plogmaker, et al., *Time-frequency representation of autoionization dynamics in helium*, J. Phys. B **51**(4), 044002 (2018).
- [10] L. Barreau, C. L. M. Petersson, M. Klinker, A. Camper, C. Marante, T. Gorman, D. Kiesewetter, L. Argenti, P. Agostini, J. González-Vázquez, et al., *Disentangling spectral phases of interfering autoionizing states from attosecond interferometric measurements*, Phys. Rev. Lett. **122**, 253203 (2019).
- [11] M. Turconi, L. Barreau, D. Busto, M. Isinger, C. Alexandridi, A. Harth, R. J. Squibb, D. Kroon, C. L. Arnold, R. Feifel, et al., *Spin-orbit-resolved spectral phase measurements around a Fano resonance*, J. Phys. B **53**(18), 184003 (2020).
- [12] L. Neoricić, D. Busto, H. Laurell, R. Weissenbilder, M. Ammitzböll, S. Luo, J. Peschel, H. Wikmark, J. Lahl, S. Maclot, et al., *Resonant two-photon ionization of helium atoms studied by attosecond interferometry*, Frontiers in Physics **10** (2022).
- [13] M. Han, H. Liang, J.-B. Ji, L. C. Sum, K. Ueda, J. M. Rost, and H. J. Wörner, *Interference control of Fano resonances and dynamical imaging of an electron wave packet*, Ultrafast Science **5**, 0091 (2025).
- [14] A. S. Kheifets, *Resonant photoionization and time delay. Topical review*, J. Phys. B **58**(7), 072001 (2025).
- [15] S. Donsa, N. Douguet, J. Burgdörfer, I. Brezinová, and L. Argenti, *Circular holographic ionization-phase meter*, Phys. Rev. Lett. **123**, 133203 (2019).
- [16] M. Han, J.-B. Ji, T. Balciunas, K. Ueda, and H. J. Wörner, *Attosecond circular-dichroism chronoscopy of electron vortices*, Nature Physics **19**, 230 (2023).
- [17] M. Han, J.-B. Ji, K. Ueda, and H. J. Wörner, *Attosecond metrology in circular polarization*, Optica **10**(8), 1044 (2023).
- [18] M. Han, J.-B. Ji, C. S. Leung, K. Ueda, and H. J. Wörner, *Separation of photoionization and measurement-induced delays*, Science Advances **10**(4), ead2629 (2024).
- [19] J. Dahlström, D. Guénot, K. Klünder, M. Gisselbrecht, J. Mauritsson, A. L. Huillier, A. Maquet, and R. Taïeb, *Theory of attosecond delays in laser-assisted photoionization*, Chem. Phys. **414**, 53 (2012).
- [20] M. Swoboda, T. Fordell, K. Klünder, J. M. Dahlström, M. Miranda, C. Buth, K. J. Schafer, J. Mauritsson, A. L’Huillier, and M. Gisselbrecht, *Phase measurement of resonant two-photon ionization in helium*, Phys. Rev. Lett. **104**, 103003 (2010).
- [21] L. Drescher, T. Witting, O. Kornilov, and M. J. J. Vrakking, *Phase dependence of resonant and antiresonant two-photon excitations*, Phys. Rev. A **105**, L011101 (2022).
- [22] A. Autuori, D. Platzter, M. Lejman, G. Gallician, L. Maëder, A. Covolo, L. Bosse, M. Dalui, D. Bresteau, J.-F. Hergott, et al., *Anisotropic dynamics of two-photon ionization: An attosecond movie of photoemission*, Science Advances **8**(12), eabl7594 (2022).
- [23] W. Jiang, L. Roantree, L. Han, J. Ji, Y. Xu, Z. Zuo, H. J. Wörner, K. Ueda, A. C. Brown, H. W. van der Hart, et al., *Heterodyne analysis of high-order partial waves in attosecond photoionization of helium*, Nature Communications **16**, 381 (2025).
- [24] M. Moiola, M. M. Popova, K. R. Hamilton, D. Ertel, D. Busto, I. Makos, M. D. Kiselev, S. N. Yudin, H. Ahmadi, C. D. Schröter, et al., *Role of intermediate resonances in attosecond photoelectron interferometry in neon*, Phys. Rev. Res. **7**, 023034 (2025).
- [25] D. M. Villeneuve, P. Hockett, M. J. J. Vrakking, and H. Niikura, *Coherent imaging of an attosecond electron wave packet*, Science **356**(6343), 1150 (2017).
- [26] A. S. Kheifets and A. W. Bray, *RABBITT phase transition across the ionization threshold*, Phys. Rev. A **103**, L011101 (2021).
- [27] A. Kheifets, *Revealing the target electronic structure with under-threshold RABBITT*, Atoms **9**(3), 66 (2021).
- [28] A. S. Kheifets, *Under-threshold RABBITT in argon*, J. Phys. B **56**(9), 095201 (2023).
- [29] A. S. Kheifets, *Characterization of XUV+IR ionization using the circular dichroic phase*, Phys. Rev. Res. **6**(1), L012002 (2024).
- [30] A. S. Kheifets, *Circularly polarized RABBITT on atomic shells with large orbital momentum*, J. Phys. B **58**(4), 045601 (2025).
- [31] D. Busto, J. Vinbladh, S. Zhong, M. Isinger, S. Nandi, S. Maclot, P. Johnsson, M. Gisselbrecht, A. L’Huillier, E. Lindroth, et al., *Fano’s propensity rule in angle-resolved attosecond pump-probe photoionization*, Phys. Rev. Lett. **123**, 133201 (2019).
- [32] D. I. R. Boll, L. Martini, A. Palacios, and O. A. Fojón, *Two-color polarization control of angularly resolved attosecond time delays*, Phys. Rev. A **107**, 043113 (2023).
- [33] M. Berkane, C. Lévesque, R. Taïeb, J. Caillat, and J. Dubois, *Probing Wigner time delays with photoelec-*

- tron interferometry: Anisotropic long-range imprint of the short-range centrifugal potential*, Phys. Rev. A **110**, 013120 (2024).
- [34] J. B. Ji, K. Ueda, M. Han, and H. J. Wörner, *Analytical expression for continuum-continuum transition amplitude of hydrogen-like atoms with angular-momentum dependence*, J. Phys. B **57**(23), 235601 (2024).
 - [35] D. I. R. Boll, A. Palacios, and O. A. Fojón, *Dalgarno-Lewis equation and its application to ultrafast two-photon processes: Short- and long-range terms for intermediate states*, Phys. Rev. A **111**, 043107 (2025).
 - [36] M. Kotur, D. Guénot, Jiménez-Galán, D. Kroon, E. W. Larsen, M. Louisy, S. Bengtsson, M. Miranda, J. Mauritsson, C. L. Arnold, et al., *Spectral phase measurement of a Fano resonance using tunable attosecond pulses*, Nature Communications **7**, 10566 (2016).
 - [37] M. Isinger, D. Busto, S. Mikaelsson, S. Zhong, C. Guo, P. Salières, C. L. Arnold, A. L’Huillier, and M. Gisselbrecht, *Accuracy and precision of the RABBIT technique*, Phil. Trans. Royal Soc. A **377**(2145), 20170475 (2019).
 - [38] L. Roantree, J. Wragg, H. van der Hart, and A. Brown, *Energy- and angle-resolved spectral phases via semirelativistic ab initio RABBITT simulations*, Phys. Rev. A **108**, 023112 (2023).
 - [39] C. Alexandridi, D. Platzter, L. Barreau, D. Busto, S. Zhong, M. Turconi, L. Neorici, H. Laurell, C. L. Arnold, A. Borot, et al., *Attosecond photoionization dynamics in the vicinity of the Cooper minima in argon*, Phys. Rev. Research **3**, L012012 (2021).
 - [40] V. J. Borràs, J. González-Vázquez, L. Argenti, and F. Martín, *Attosecond photoionization delays in the vicinity of molecular feshbach resonances*, Science Advances **9**(15), eade3855 (2023).
 - [41] S. Patchkovskii and H. Muller, *Simple, accurate, and efficient implementation of 1-electron atomic time-dependent Schrödinger equation in spherical coordinates*, Computer Physics Communications **199**, 153 (2016).
 - [42] V. Serov, *Time-dependent convergent close coupling method for molecular ionization in laser fields*, arXiv preprint arXiv:2405.12455 (2024).
 - [43] J. Itatani, F. Quéré, G. L. Yudin, M. Y. Ivanov, F. Krausz, and P. B. Corkum, *Attosecond streak camera*, Phys. Rev. Lett. **88**, 173903 (2002).
 - [44] L. Tao and A. Scrinzi, *Photo-electron momentum spectra from minimal volumes: the time-dependent surface flux method*, New J. Phys. **14**, 013021 (2012).
 - [45] F. Morales, T. Bredtmann, and S. Patchkovskii, *iSURF: a family of infinite-time surface flux methods*, J. Phys. B **49**(24), 245001 (2016).
 - [46] V. V. Serov, V. L. Derbov, T. A. Sergeeva, and S. I. Vinitzky, *Hybrid surface-flux method for extraction of the ionization amplitude from the calculated wave function*, Phys. Rev. A **88**, 043403 (2013).
 - [47] A. A. Krylovetsky, N. L. Manakov, and S. I. Marmo, *Generalized sturm expansions of the Coulomb Green’s function and two-photon gordon formulas*, Sov. Phys. – JETP **92**, 37 (2001).
 - [48] P. Virtanen, R. Gommers, T. E. Oliphant, M. Haberland, T. Reddy, D. Cournapeau, E. Burovski, P. Peterson, W. Weckesser, J. Bright, et al., *SciPy 1.0: Fundamental Algorithms for Scientific Computing in Python*, Nature Methods **17**, 261 (2020).
 - [49] *A Python library for arbitrary-precision floating-point arithmetic (version 1.3.0)* (2023), <http://mpmath.org/>.